Journal of Polymer Research (2020) 27: 312
https://doi.org/10.1007/s10965-020-02276-1

ORIGINAL PAPER

Functionalized carbon dot nanoparticles reinforced soy protein isolate biopolymeric film

Shikha Rani[1] · K. Dinesh Kumar[2] · Saptarshi Mandal[3] · Rakesh Kumar[1]

Received: 5 February 2020 / Accepted: 3 September 2020 / Published online: 28 September 2020

Abstract

Amine and carboxyl functionalized carbon dots (CDs), i.e., citric acid polyethylenimine (CPI) and citric acid glycine (CCG) at different contents (0.05 to 0.5% w/w with respect to soy protein isolate (SPI)) were incorporated in glycerol plasticized SPI to produce CDs reinforced SPI films. Functionalized CDs were characterized by fluorescence spectroscopy and X-ray diffraction (XRD). The CDs reinforced SPI films were structurally, morphologically, and mechanically characterized by Fourier transform infrared (FTIR) spectroscopy, scanning electron microscope (SEM) and mechanical properties, respectively. Water uptake studies were also carried out for CDs reinforced SPI films. The results from FTIR study indicated shifting of amide II band from 1544 to 1530 cm^{-1} for CPI incorporated SPI and generation of a band at 1741 cm^{-1} for CCG incorporated SPI indicating unbounded –COOH groups of CCG with SPI. The tensile stress and tensile modulus of CPI, as well as CCG reinforced SPI films increased, indicating reinforcement effect of CDs on SPI film. The maximum tensile stress of 0.5% CPI and 0.15% CCG loaded SPI was nearly 38.03% and 42.85% higher than the maximum tensile stress of neat SPI film. Antibacterial activity of CPI and CCG reinforced SPI films against *E. coli* and *L. monocytogenes* were also studied but CCG and CPI incorporated SPI films did not show any inhibitory effect on above mentioned bacteria. This work will be helpful in fabricating functionalized CDs reinforced SPI film from the renewable resources with low water uptake and good mechanical properties.

Keyword Soy protein isolate · Functionalized carbon dots · Reinforcement · Tensile properties · Biofilms · Water uptake

Introduction

Synthetic plastics are major threat for environment in this era because of their immortal nature [1]. Increasing demand for plastic materials is only adding more and more load of synthetic plastic-based pollutants to environment. Researchers are trying to find out the appropriate alternative materials from starch, cellulose, chitin/chitosan, protein, etc. so that one time usages of synthetic plastics can be reduced [2–6]. Materials prepared from soy protein isolate (SPI) can be one of the replacements of synthetic based plastics. SPI being a protein macromolecule is naturally degradable, biocompatible, easily available, and possesses a very good film-forming capacity. Due to these properties, SPI is a very suitable candidate for packaging applications, edible films, food material, biodegradable implants [7, 8], composite films [9, 10], composite beads [11], nanofabric for removing airborne pollutants [12, 13], etc. The addition of nanofillers into a polymer matrix results in an improvement in the properties of natural polymers including enhanced mechanical [14], thermal, barrier [15] and physicochemical properties [16].

However, apart from the good film-forming capacity, excessive water sensitivity is a major hindrance, which limits the acceptance of SPI based plastics on a commodity basis. To minimize the water uptake and to increase the mechanical properties of SPI based materials, different approaches such as addition of other biopolymers, flavonoids, polyphenols, and nanoparticles are adopted [17–20]. The incorporation of these additives might trigger antimicrobial properties or antioxidant properties as well as increase in mechanical properties of the as-prepared SPI films.

✉ Rakesh Kumar
krrakesh72@gmail.com; rakeshkr@cusb.ac.in

[1] Department of Biotechnology, Central University of South Bihar, Gaya 824236, India

[2] Department of Materials Science & Engineering, Indian Institute of Technology, Patna 801106, India

[3] Department of Chemistry, Indian Institute of Technology, Patna 801106, India

Nano reinforcement is quite demanding and attractive strategies for the fabrication of modified SPI based films with improved properties. Xiang et al. used acid-treated carbon nanotubes (CNTs) as reinforcing fillers for SPI matrices, and the reinforced biopolymeric film showed excellent properties [21]. Some nanofillers such as industrial lignin [22], layered silicate [23, 24], carbon nanoparticles (CNP) [18], ZnS nanoparticles [25], $Cu_3(PO_4)_2{\cdot}3H_2O$ [26], and citric acid-modified starch nanoparticles (CSN) [27] showed promising effect upon reinforcement in SPI films as compared to neat SPI films. Besides several nanoparticles, functionalized CNP secures a specific space in the fabrication of SPI film due to their water soluble nature and presence of functional groups on the surface. In charged nanoparticles such as functionalized CNP, a large number of –OH and –COOH groups are exposed on the surface which may interact well with $-NH_2$, -OH and -COOH of protein. Indeed, these interactions may strengthen the overall performance of functionalized CNP incorporated SPI film [18]. The mechanical properties, water resistance, thermal stability, etc. of the resulting protein-based composite films got dramatically enhanced by the incorporation of CNP in SPI [18].

Carbon dots (CDs), a carbonaceous nanomaterial with a size less than 10 nm, have attracted tremendous attention in recent times because of its many fascinating prospects like negligible photo-bleaching, excellent water solubility, good biocompatibility, and excellent chemical stability, etc.[28, 29]. The overabundance of surface functional groups on the surface of CDs exhibited so much flexibility that it eventually dynamize the emergence of CDs as a nanofiller in the polymer matrix. From advancing the physico-mechanical properties to a zing like fluorescent, antimicrobial, or photocatalytic activity of CDs-reinforced polymers, all originated from the boon of the extrinsic and intrinsic nature of the CDs [30–32].

In our study, we have synthesized amine and carboxyl functionalized CDs, i.e., citric acid polyethylenimine (CPI) and citric acid glycine (CCG) with the precursor citric acid, polyethylenimine, and glycine. The CDs were characterized by fluorescence spectroscopy and XRD. CDs were then incorporated in SPI to fabricate reinforced biofilms. The as-prepared biofilms were structurally and morphologically characterized by Fourier transform infrared (FTIR) spectroscopy and scanning electron microscope (SEM), respectively. Mechanical, water uptake, antibacterial, and transmittance studies of CCG and CPI reinforced SPI biofilms were also carried out. Two different nitrogen precursors were used to assess the variative roles of surface functional groups of CDs towards SPI.

Materials and methods

Materials

Soy protein isolate with a purity of 90.27% (on dry basis) was purchased from Zhenghou Ruikang Enterprise Co., Ltd. (Zhengzhou, China). Citric acid monohydrate, glycine, 1-(3-dimethylaminopropyl)-3-ethylcarbodiimide hydrochloride (EDC.HCl) and N-hydroxysuccinimide (NHS) were obtained from Alfa Aesar, Hyderabad, India. All chemicals were used as received. Nanopure water from millipore was used in the synthesis of CDs. Glycerol from Fisher Scientific, sodium hydroxide pellets from Titan Biotech Ltd. and Luria Bertani (LB) powder from HiMedia, were used in the experiments. *E. Coli* /BL21strain was obtained from Gbiosciences. *L. monocytogenes* MTCC 839 was supplied by IMTECH Chandigarh, India.

Synthesis of CCG and CPI

CCG and CPI were synthesized following previously reported methods with slight modifications [33, 34]. In a facile approach, citric acid (10 mmol) and glycine (10 mmol) were dissolved in 20 ml of water and heating was done at 120 °C for 16 h to obtain a brownish mass. After cooling to room temperature, water was added to it to disperse the mass and pH was adjusted to 7.4 with NaOH solution. The resulting solution was then passed through a 0.22 µm nylon syringe filter to remove the undissolved or large agglomerated particles. The brownish-yellow CCG solution was stored at 4 °C for further use. Similarly, CPI was synthesized by pyrolysis of 1 g of citric acid and 0.5 g of polyethylenimine. CPI and CCG nanoparticles in liquid form have the solid content of 0.06% and 0.04%. The morphology and average size of pristine CPI and CCG was reported as spherical and 2–4 nm, respectively [33, 34].

Preparation of neat and carbon dot nanoparticles incorporated SPI film

SPI (6%) with glycerol as plasticizer has been used to prepare SPI films by solution casting method. Firstly 0.9 g of glycerol (30% w/w of SPI) was added in 50 ml distilled water followed by addition of 3 g of SPI to distilled water bit by bit in stirring condition to get SPI suspension. The temperature of SPI suspension was maintained at 60 °C, and dilute NaOH solution (1 ml of 1 M NaOH solution) was added to the SPI suspension to adjust the pH value of 9–9.5. Subsequently, the SPI suspension was kept at 60 °C for 1 h at stirring condition followed by 3–4 h in vacuum desiccators to remove air bubbles. The SPI suspension (free from

air bubbles) was poured on glass plates having a dimension of 15 cm × 10 cm and was allowed to dry at 55–60 °C for 24 h. To peel-off the SPI film from glass plate, plates were first transferred in desiccators with RH of 75%, which eventually makes SPI film elastic enough to be peeled-off from the glass plate.

CCG and CPI incorporated SPI film were prepared by the same method as discussed above with slight modifications. For the fabrication of CCG and CPI incorporated SPI films, SPI suspension was first heated and stirred for 30 min, and after that, the required contents of CCG (0.05%, 0.1%, 0.15% and 0.2% CCG w/w of SPI) and CPI (0.1%, 0.3% and 0.5% of CPI w/w of SPI) were added in the SPI suspension maintaining the temperature of 60 °C and stirred for another 30 min. The SPI films prepared at different contents of CCG were designated as S-0CCG, S-0.05CCG, S-0.1CCG, S-0.15CCG, S-0.2CCG, and the CPI containing SPI films were designated as S-0CPI, S-0.1CPI, S-0.3CPI, S-0.5CPI. The numeric value in the designation of sample films denotes the percentage contents of additives.

Antibacterial studies

E. coli (Gram-negative bacteria) and *L. monocytogenes* (Gram-positive bacteria) were used to check the antibacterial properties of CCG and CPI reinforced SPI films. Both the bacteria were revived using 10 ml of LB broth by incubation of bacteria containing broth on a shaker incubator. When the optical density (OD) of broth reached 0.4, 10 µl (3.2×10^4 bacteria) of *E. coli* and *L. monocytogenes* culture was taken and spread on respective plates separately for each concentration of CCG and CPI containing SPI film. The experiments were performed in triplicates. Neat, CCG, and CPI incorporated SPI films (1 cm × 1 cm) were then positioned on each of the respective plates. After that, plates were transferred on a static incubator for overnight incubation at 37 °C. Plates were observed after incubation for the growth of bacteria.

Characterizations

Powder X-ray diffraction analysis for CCG and CPI was carried out in a Rigaku TTRX-III diffractometer with Cu-Kα (λ = 1.54 Å) as an X-ray source. Steady-state fluorescence measurement for CCG and CPI was performed with a Fluoromax-4P spectrofluorometer (Horiba Jobin Yvon) at room temperature. Transmission electron microscopy (TEM) was performed for CCG and CPI and captured on a Hitachi (H-7500) electron microscope at an accelerating voltage of 100 kV. For TEM, the samples were prepared by dispersing 10 ml solution of CCG and CPI (0.5 mg/l) on a carbon grid and air-dried for 20 min for imaging by TEM unit.

CCG and CPI incorporated SPI films were scanned at room temperature from 4000 to 400 cm^{-1} (wavenumber) with a resolution of 4 cm^{-1} on FTIR spectrophotometer from Perkin-Elmer, USA. An average of 32 scans was used to report the spectra.

Tensile properties including tensile stress, Young's modulus, and elongation at break of neat SPI film as well as CCG and CPI nanoparticles incorporated SPI films were reported as per ASTM D 882. The tensile tests were performed on a Universal Tensile Testing machine from Zwick, Germany. Five tests were performed for each specimen having dimension of 8 cm × 1 cm with a thickness of ~ 0.2 mm and cross head speed of 10 mm/min. 10 kN load cell was used for the measurement.

Cross-section morphology of neat SPI film as well as CCG and CPI incorporated SPI films were carried out by SEM (EVO-SEM 15/18 (Carl Zeiss Microscopy, Ltd)) at an accelerating voltage of 20 kV. The samples were coated with gold prior to subjecting it to morphology experiment. Water uptake experiment in triplets was carried as per ASTM D570-81. For this experiment, SPI film strips at all the different contents of CCG and CPI were cut in a dimension of 1 cm x 1 cm and dried at 60 °C for 24 h in an incubator. After drying, the samples were cooled in desiccators maintained at 0% RH with silica beads for 1 h, and initial weight (W_0) of the cooled samples was taken. Separate plastic container for each strip was labeled, and filled with distilled water. The sample strips were dipped in it and left undisturbed for 24 h. Afterward, the strips were taken out carefully from the bottle wiped with tissue paper for removal of excess water and weighed again to get final weight (W_1). The difference in the final and initial weight is the value of water uptake, and the percentage water uptake is calculated by the formula given below.

$$WaterUptake(\%) = \frac{W_1 - W_0}{W_0} \times 100$$

Results and discussions

Characterization of CCG and CPI

Pyrolysis of citric acid, along with nitrogen precursor, often produces CDs with strong fluorescence. Herein, we have used two different nitrogen precursors, glycine and polyethylenimine for the synthesis of CCG and CPI, respectively, to vary the number of functional groups on the surface of CDs. X-ray diffraction analysis reveals typical diffraction peak at 26° for CCG and at 28° for CPI (Fig. 1a, 1b) that correspond to (002) plane of a graphitic framework, which confirmed the successful carbonization

of the precursors. The weak and broad diffraction peak discloses the partial graphitization and a highly disordered carbon framework [35]. Both CCG and CPI exhibit blue fluorescence and steady-state fluorescence analysis was performed to decipher that. It reveals excitation dependent fluorescence emission for CCG and excitation independent fluorescence emission for CPI (Fig. 2a, 2b). Figure 3 shows the TEM images of CCG and CPI with the size distribution ranging from 2 to 6 nm in diameter. The generalized structure of CPI and CCG is given in Fig. 4 [33–35].

FTIR

Figure 5 and Fig. 6 show the FTIR spectra of CPI and CCG incorporated SPI films, respectively. In this spectra, a broad band between 3200 and 3300 cm^{-1} is generated due to N–H stretching and is assigned as amide A of neat soy protein films. The peak at 1639 cm^{-1} is attributed to amide I band of protein vibration, and that is attributed to C = O stretching. The peak at 1544 cm^{-1} is attributed to amide II bands of protein due to interaction between -CN stretching and -NH bending of SPI [25]. The peak at 1261 cm^{-1} also

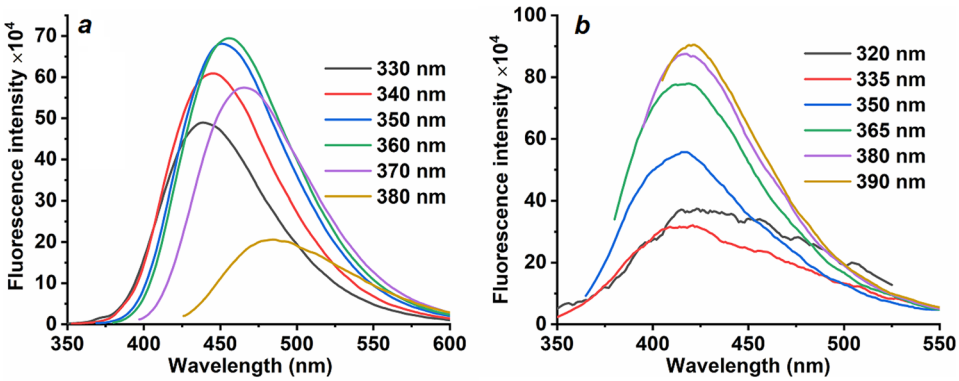

Fig. 1 Fluorescence spectra of (a) CCG and (b) CPI

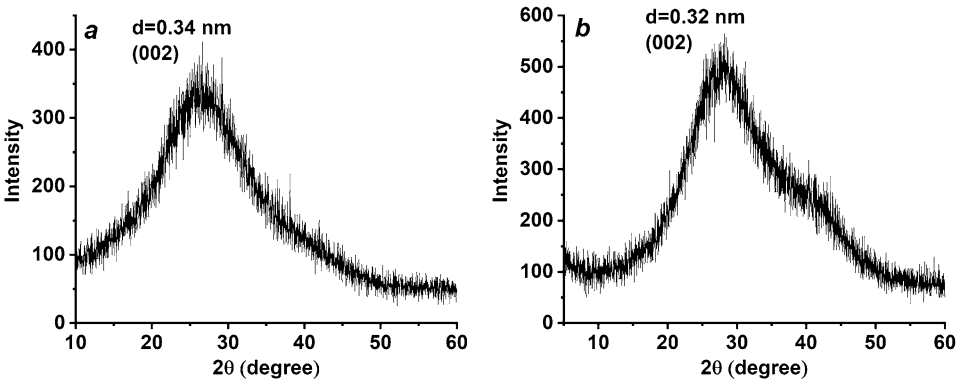

Fig. 2 X-ray diffraction patterns of (a) CCG and (b) CPI

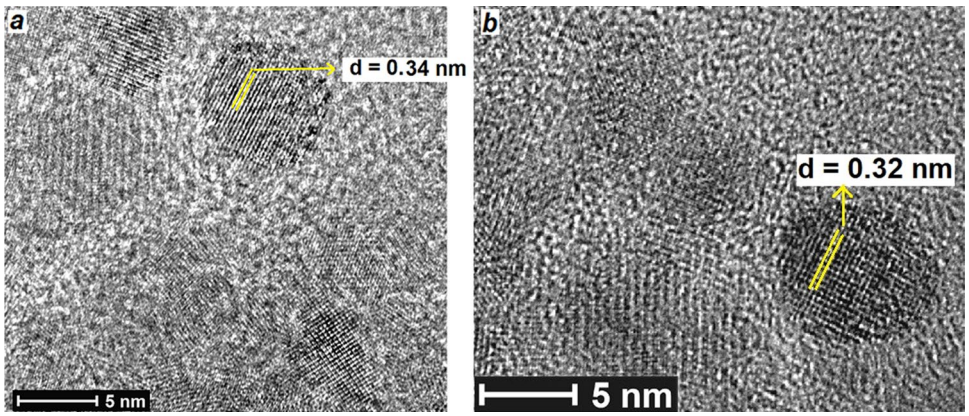

Fig. 3 TEM of (a) CCG and (b) CPI

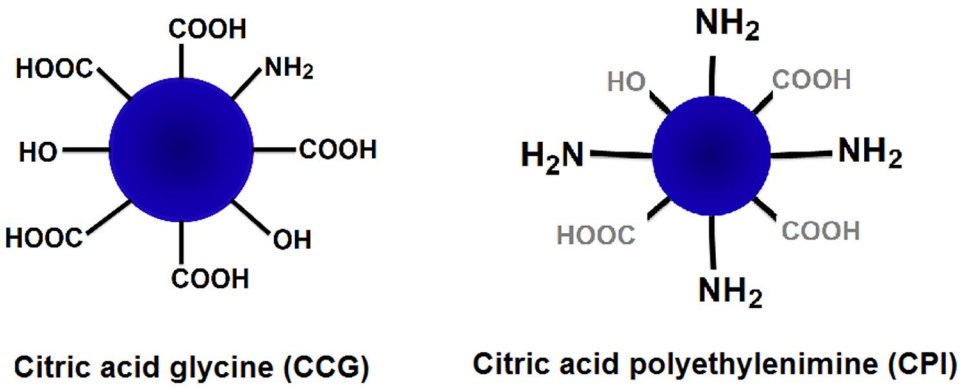

Fig. 4 Generalized structure of CCG and CPI

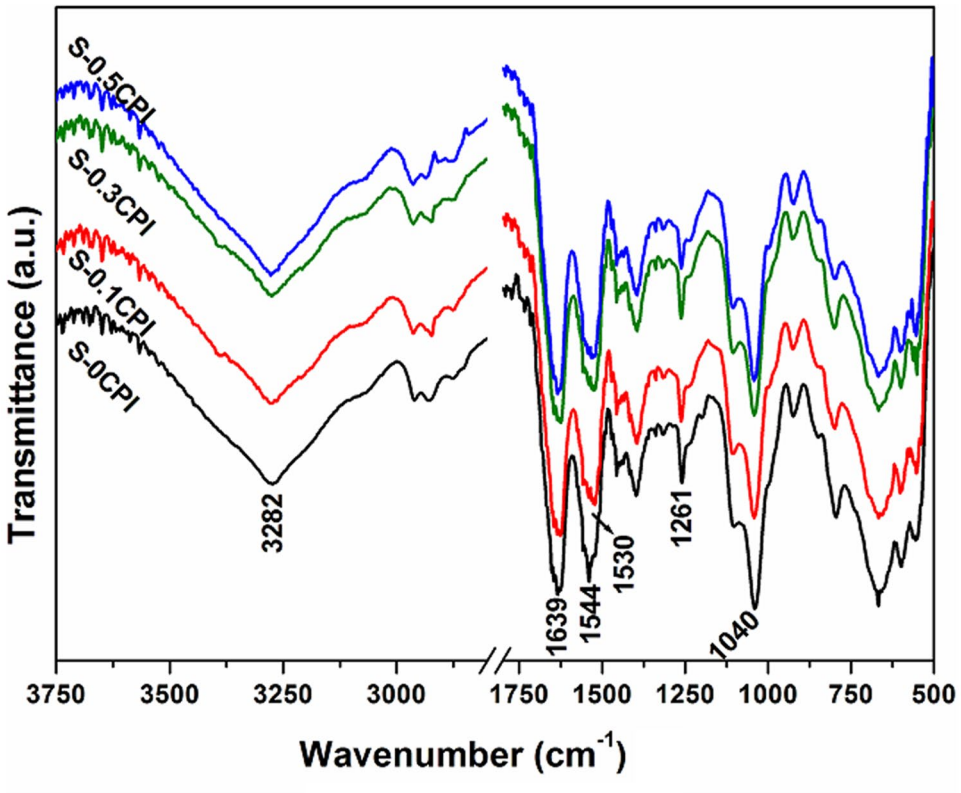

Fig. 5 FTIR spectra of CPI incorporated SPI films

represents the interaction between -CN stretching and -NH bending and is attributed to amide III band. After incorporation of CPI, the band shifts to 1530 cm^{-1}, which may be due to interaction between -CN stretching and -NH bending of CPI, as shown structurally in Fig. 5. The intensity of band at 1261 cm^{-1} increase after incorporation of CCG in SPI films (Fig. 6). In addition, a band at 1741 cm^{-1} is also observed for S-0.15CCG and S-0.2CCG, which is attributed to C = O stretching of carboxylic group [33]. The generation of band at 1741 cm^{-1} indicates abundance of unbounded –COOH groups at higher contents of CCG. On the other hand, -COOH groups interact with amine group of SPI at lower content of CCG, i.e., for S-0.05CCG and S-0.1CCG in CCG incorporated SPI film.

Mechanical properties

Figure 7 shows the mechanical properties of CPI incorporated SPI film. The tensile strength and tensile modulus of CPI incorporated SPI films increase from 5.18 MPa to 7.15 MPa and 28.85 MPa to 68.7 MPa, respectively in case of 0.5% CPI incorporated SPI films. Tensile modulus of SPI films increases from 28.85 MPa to 84.7 MPa for 0.1% CPI incorporated SPI film. After that, modulus decreases to

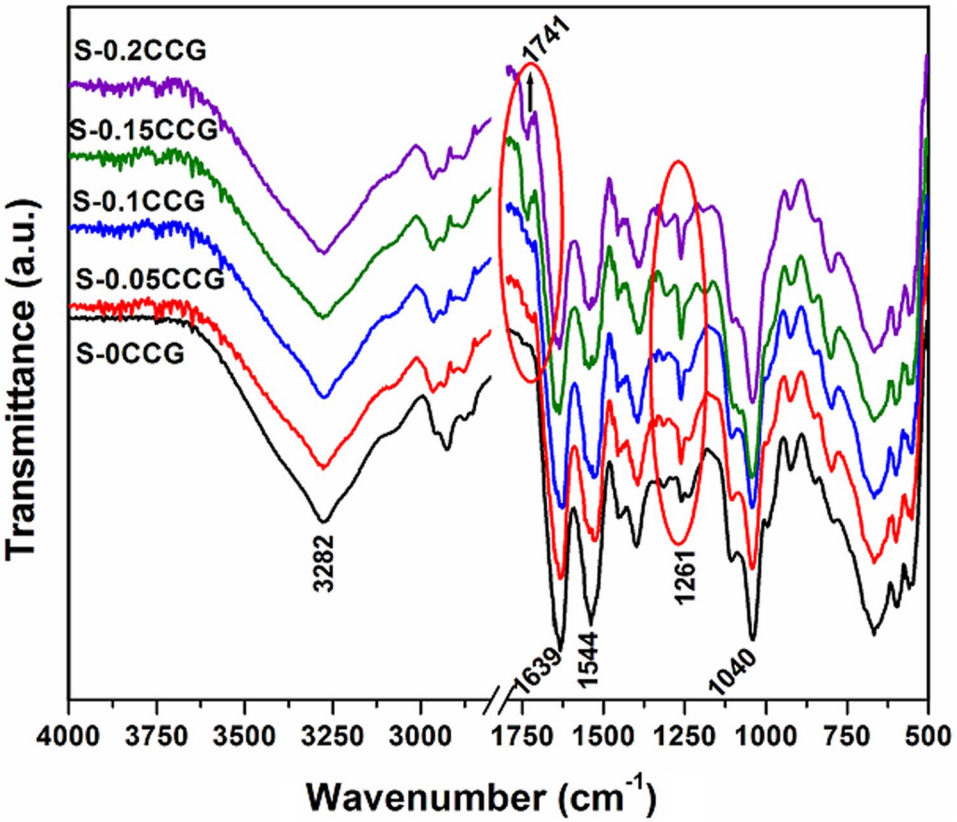

Fig. 6 FTIR spectra of CCG incorporated SPI films

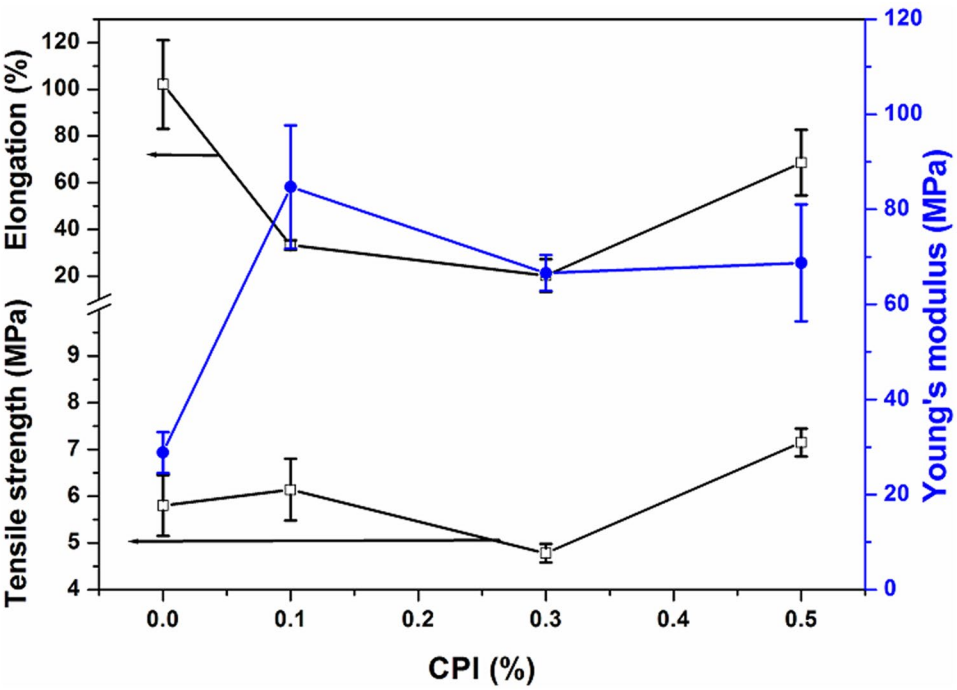

Fig. 7 Mechanical properties of CPI incorporated SPI films

68.7 MPa in case of 0.5% CPI incorporated SPI films. Elongation at break decreases from 102.07% to 68.6% in case of 0.5% CPI incorporated SPI film. These findings indicate that higher mechanical properties are observed for CPI reinforced SPI film. As from the structure of CPI (Fig. 4), there are various functional groups exposed on the surface

of nanomaterial, which leads to better interaction with SPI matrix at 0.5% concentration of CPI. And tensile strength results also indicate that the optimum concentration of CPI in SPI could be 0.5%.

Figure 8 shows the mechanical properties of CCG incorporated SPI film. The tensile strength and tensile modulus increase from 5.18 MPa to 7.4 MPa and 28.85 MPa to 115 MPa, respectively for 0.15% CCG incorporated SPI films. At higher content of CCG, i.e., 0.2% in SPI, tensile strength and tensile modulus decrease. Interestingly, the elongation at break decreases from 102.07% to 7.87% for 0.15% CCG incorporated films. Li et al. have also reported the increase in the mechanical properties of SPI biofilms after incorporating CNP [18]. This result indicated that at 0.15% concentration of CCG, there is presence of sufficient exposed surface functional groups (Fig. 4) which interacted well with exposed functional groups of SPI matrix. However, at 0.2% concentration of CCG, there may be self-aggregation of nanomaterial that leads to decrease in mechanical strength [18].

These results indicate that reinforcement of CCG and CPI in SPI matrix enhances the mechanical properties of reinforced film. Li et al. have also reported the increase in the mechanical properties of SPI biofilms after incorporating CNP [18]. According to Lu et al. CNP interacts strongly with SPI matrix, due to which the motion of the matrix get restricted [36]. Also with decreasing size of nanomaterial, the surface atom gets unsaturated for the lack of the neighboring atoms. Huge number of dangling bond could be produced due to intrinsic defaults contained by the CNP. Those dangling bonds are highly reactive and contain strong affinity for functional groups in SPI (NH_2, OH and COOH) and could form hydrogen bond with them. This explanation defines the increased mechanical strength of prepared CCG and CPI incorporated SPI films [18].

Water uptake

Figure 9 shows the water uptake properties of CCG and CPI incorporated SPI films. The water uptake data of CCG and CPI incorporated SPI film shows that water resistance of the as-prepared SPI films increases after incorporation of CCG and CPI. Neat SPI film shows water uptake of 159.95% while the CCG and CPI incorporated biofilms show a decrease in water uptake (~ 58 ± 3%) except for S-0.2CCG. The decrease in water uptake values may be attributed to the hydrogen bonding of functional groups of SPI with exposed carboxyl, amine, and polyethylenimine functional groups of CCG and CPI. It has been shown in FTIR section that S-0.15CCG and S-0.2CCG contain a large number of unbounded –COOH groups, and due to presence of these unbounded –COOH groups, the water uptake is higher than that of S-0.05CCG and S-0.1CCG.

Morphology

Figure 10 shows the SEM image of neat, CCG, and CPI incorporated SPI films. The neat SPI film exhibits a relatively less coarse surface. In S-0.3CPI and S-0.2CCG, the obvious change of cross sections can be observed as more

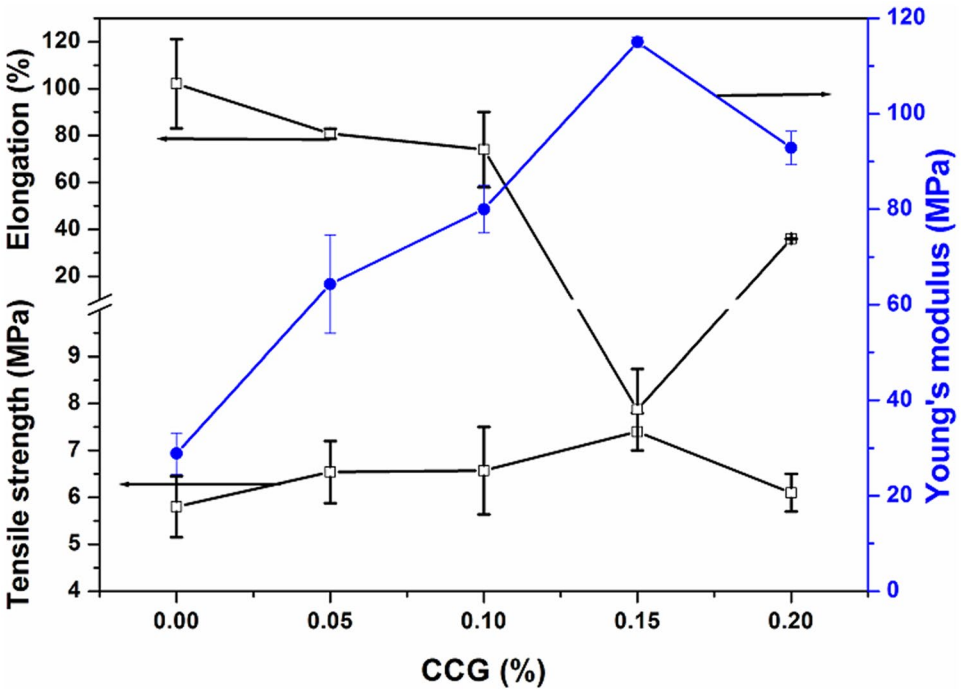

Fig. 8 Mechanical properties of CCG incorporated SPI films

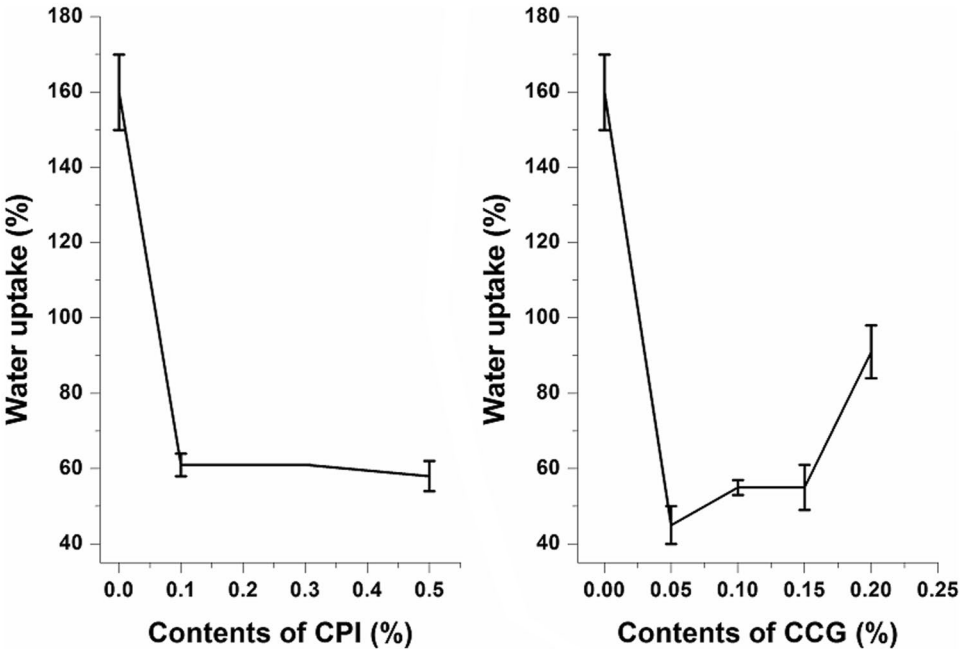

Fig. 9 Water uptake (%) of CPI and CCG incorporated SPI films

coarse and crack structure, and this change is not obvious for S-0.1CPI and S-0.1CCG because only a small amount of CPI and CCG are dispersed in SPI matrix. The original structure of SPI is weakly destroyed at high contents of CPI and CCG in SPI matrix [18].

Interaction of CPI and CCG with SPI

Based on the results obtained above, mode of interactions of CPI and CCG with SPI has been discussed here. Electrostatic attractions and different weak non-covalent bondings (H-bond, van der Waals forces of attraction) are involved in interaction between SPI and CDs. CPI has larger number of amines on the surface of CDs as compared to that of CCG where carboxyl groups predominate (Fig. 4). As reported in literature, charged nanoparticles such as functionalized CNP, a large number of–OH, -NH_2 and –COOH groups present in CCG and CPI are exposed out on the surface, and that may interact with -NH_2, -OH and -COOH of SPI. These interactions strengthen the overall performance of CDs incorporated SPI biofilm and role of these functional groups is clearly visible in terms of high mechanical properties (Fig. 7 and Fig. 8) and low water uptake (Fig. 9) [18].

Antibacterial properties

Interestingly, few CDs exhibited excellent antibacterial properties [37]. Hence, it is worth to study the antibacterial properties of CPI and CCG incorporated SPI biofilms. The antibacterial results indicate that CPI and CCG incorporated SPI films cannot form the zone of inhibition against against *E. coli* and *L. monocytogenes*, and the bacteria grow on the surface of film after 24 h (Figures not shown). So we can say that CPI and CCG incorporated SPI biofilms do not have antibacterial properties. These biofilms can be easily degraded in the presence of bacteria.

Conclusions

CCG and CPI having dimension 0.34 nm and 0.32 nm (as obtained by XRD) were successfully synthesized. Also, functionalized CDs (CCG and CPI) incorporated SPI-based biofilms with improved properties were successfully fabricated. It has been observed from FTIR study that CCG incorporated SPI films showed high amount of –COOH groups which is not bounded with SPI. The biofilms reinforced by CPI and CCG showed higher water resistance in addition to better mechanical properties as compared to neat SPI films. The tensile stress and tensile modulus for CCG and CPI incorporated SPI biofilms increased from 5.80 MPa to ~ 7.5 MPa and 28.85 MPa to ~ 115 MPa, respectively. Interestingly, the reinforcement effect by CPI and CCG in SPI was observed at low contents of CPI (0.5%) and CCG (0.15%). This may be attributed to the presence of -COOH and -NH_2 functional groups in CDs that may interact with the functional groups present on the surface of SPI material, and this interaction in turn strengthen the material properties of the SPI biofilms. *E. coli* and *L. monocytogenes* could easily grow on CDs incorporated biofilms indicating biodegradable nature of CDs reinforced SPI films.

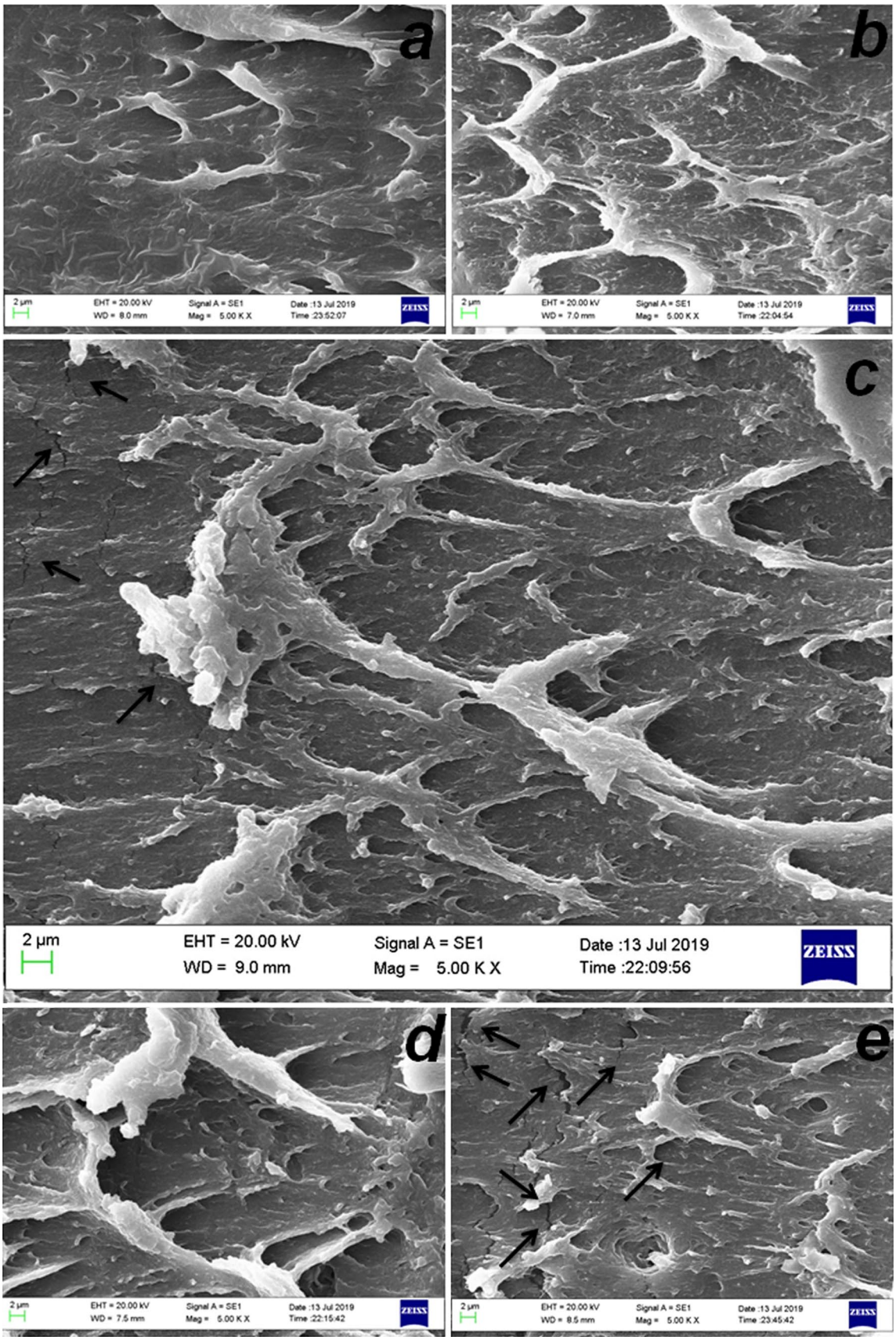

Fig. 10 Cross-section morphology of (a) 0% (b) 0.1% (c) 0.3% CPI (d) 0.1% (e) 0.2% CCG incorporated SPI films

References

1. Yin GZ, Yang XM (2020) Biodegradable polymers: a cure for the planet, but a long way to go. J Polym Res 27:38
2. Jagadeesh D, Reddy DJP, Rajulu AV (2011) Preparation, and properties of biodegradable films from wheat protein isolate. J Polym Environ 19:248–253
3. Ma ZS, Liu DG, Zhu Y, Li ZH, Li ZX, Tian HF, Liu HQ (2016) Graphene oxide/chitin nanofibril composite foams as column adsorbents for aqueous pollutants. Carbohydr Polym 144:230–237
4. Qu L, Chen G, Dong S, Huo Y, Yin Z, Li S, Chen Y (2019) Improved mechanical and antimicrobial properties of zein/chitosan films by adding highly dispersed nano-TiO_2. Ind Crops Prod 130:450–458
5. Muthulakshmi L, Rajini N, Nellaiah H, Kathiresan T, Jawaid M, Rajulu AV (2017) Preparation and properties of cellulose nanocomposite films with in situ generated copper nanoparticles using Terminalia catappa leaf extract. Int J Biol Macromol 95:1064–1071
6. Tian H, Guo G, Fu X, Yao Y, Yuan L, Xiang A (2018) Fabrication, properties and applications of soy-protein-based materials: a review. Int J Biol Macromol 120:475–490
7. Mkandawire M, Aryee AN (2018) Resurfacing and modernization of edible packaging material technology. Curr Opin Food Sci 19:104–112
8. Zhao Y, He M, Zhao L, Wang S, Li Y, Gan L, Li M, Xu L, Chang PR, Anderson DP, Chen Y (2016) Epichlorohydrin-Cross-linked hydroxyethyl cellulose/soy protein isolate composite films as biocompatible and biodegradable implants for tissue engineering. Appl Mater Interfaces 8:2781–2795
9. Wang L, Li J, Zhang S, Shi J (2016) Preparation and characterization of all-biomass soy protein isolate-based films enhanced by epoxy castor oil acid sodium and hydroxypropyl cellulose. Materials 9:193
10. Saenghirunwattana P, Noomhorm A, Rungsardthong V (2014) Mechanical properties of soy protein based "green" composites reinforced with surface modified cornhusk fiber. Ind Crops Prod 60:44–150
11. Liu F, Zou HL, Hu JW, Liu HB, Peng JB, Chen YW, Lu FH, Huo YP (2016) Fast removal of methylene blue from aqueous solution using porous soy protein isolate based composite beads. Chem Eng J 287:410–418
12. Souzandeh H, Johnson KS, Wang Y, Bhamidipaty K, Zhong WH (2016) Soy- protein based nanofabrics for highly efficient and multifunctional air filtration. Appl Mater Interfaces 8(31):20023–20031
13. Tian H, Fu X, Zheng M, Wang Y, Li Y, Xiang A, Zhong WH (2018) Natural polypeptides treat pollution complex: Moisture-resistant multi-functional protein nanofabrics for sustainable air filtration. Nano Res 11(8):4265–4277
14. Tunc S, Duman O, Polat TG (2016) Effects of montmorillonite on properties of methyl cellulose/carvacrol based active antimicrobial nanocomposites. Carbohydr Polym 150:259–268
15. Tunç S, Duman O (2011) Preparation of active antimicrobial methyl cellulose/carvacrol/montmorillonitenanocomposite films and investigation of carvacrol release. LWT-Food Sci Technol 44(2):465–472
16. Tunç S, Duman O (2010) Preparation and characterization of biodegradable methyl cellulose/montmorillonite nanocomposite films. Appl Clay Sci 48(3):414–424
17. Guo G, Tian H, Wu Q (2019) Nanoclay incorporation into soy protein/polyvinyl alcohol blends to enhance the mechanical and barrier properties. Polym Compos 40:3768–3776
18. Li Y, Chen H, Dong YM, Li K, Li L, Li JZ (2016) Carbon nanoparticles/soy protein isolate bio-films with excellent mechanical and water barrier properties. Ind Crop Prod 82:133–140
19. Han YY, Wang LJ (2016) Improved water barrier and mechanical properties of soy protein isolate films by incorporation of SiO_2 nanoparticles. RSC Adv 6(113):112317–112324
20. Rani S, Kumar R (2019) A review on material and antimicrobial properties of soy protein isolate film. J Polym Environ 27(8):1–16
21. Xiang A, Guo G, Tian H (2017) Fabrication and properties of acid treated carbon nanotubes reinforced soy protein nanocomposites. J Polym Environ 25(3):519–525
22. Huang J, Zhang L, Chen P (2003) Effects of lignin as a filler on properties of soy protein plastics II Alkaline lignin. J Appl Polym Sci 88(14):3291–3297
23. Chen P, Zhang L (2006) Interaction and properties of highly exfoliated soy protein/montmorillonite nanocomposites. Biomacromol 7(6):1700–1706
24. Yu J, Cui G, Wei M, Huang J (2007) Facile exfoliation of rectoritenanoplatelets in soy protein matrix and reinforced bionanocomposites thereof. J Appl Polym Sci 104(5):3367–3377
25. Kumar R, Anjum KA, Rani S, Sharma K, Tiwary KP, Kumar KD (2019) Material properties of ZnS nanoparticlesincorporated soy protein isolate biopolymeric film. Plast Rubb Compos 48(10):448–455
26. Xie WY, Song F, Wang XL, Wang YZ (2016) Development of copper phosphate nanoflowers on soy protein toward a superhydrophobic and self-cleaning film. ACS Sustain Chem Eng 5(1):869–875
27. Tian H, Xu G (2011) Processing and characterization of glycerol-plasticized soy protein plastics reinforced with citric acid-modified starch nanoparticles. J Polym Environ 19(3):582–588
28. Lim SY, Shen W, Gao Z (2015) Carbon quantum dots and their applications. Chem Soc Rev 44:362–368
29. Yang Z, Li Z, Xu M, Ma Y, Zhang J, Su Y, Gao F, Wei H, Zhang L (2013) Controllable synthesis of fluorescent carbon dots and their detection application as nanoprobes. Nanomicro Lett 5:247–259
30. Zhou Y, Sharma SK, Peng Z, Leblanc RM (2017) Polymers in carbon dots: A review. Polymers (Basel) 9:67
31. Ganguly S, Das P, Banerjee S, Das NC (2019) Advancement in science and technology of carbon dot-polymer hybrid composites: A review. Funct Compos Struct 1:022001
32. Duarah R, Karak N (2019) hyperbranched polyurethane/palladium-reduced carbon dot nanocomposite: an efficient and reusable mesoporous catalyst for visible-light-driven C-C coupling reactions. Ind Eng Chem Res 58:16307–16319
33. Kumari S, Solanki A, Mandal S, Subramanyam D, Das P (2018) Creation of linear carbon dot array with improved optical properties through controlled covalent conjugation with DNA. Bioconjugate Chem 29(5):1500–1504
34. Sreenath PR, Singh S, Satyanarayana MS, Das P, Kumar KD (2017) Carbon dot–Unique reinforcing filler for polymer with special reference to physico-mechanical properties. Polymer 112:189–200
35. Mandal S, Das P (2019) Ultrasensitive visual detection of mycotoxin citrinin with yellow-light emitting carbon dot and congo red. Food Chem 312:126076
36. Lu Y, Weng L, Zhang L (2004) Morphology and properties of soy protein isolate thermoplastics reinforced with chitin whiskers. Biomacromol 5:1046–1051
37. Chung YJ, Kim J, Park CB (2020) Photonic carbon dots as an emerging nanoagent for biomedical and healthcare applications. ACS Nano 14:6470–6497